January 2014

Characterization Of The Effect Of Braf Inhibitors On Melanoma Metabolism In Vitro And In Vivo

Alexander Marzuka
Yale School of Medicine, alexander.marzuka@yale.edu

Characterization of the effect of BRAF inhibitors on melanoma metabolism *in vitro* and *in vivo*

Abstract

Vemurafenib is the first FDA-approved personalized treatment for metastatic melanoma to show an improvement in survival. This serine threonine kinase inhibitor targets the mutated BRAF V600E protein, which occurs in approximately 50% of melanomas. The downstream effect of BRAF V600E blockade is inhibition of cell proliferation. Little is known about the effect of vemurafenib on glucose metabolism in melanoma cells. The Warburg effect, or the use aerobic glycolysis to generate energy and building blocks for cell proliferation, is a hallmark of cancer. Normal cells, in contrast, metabolize glucose through oxidative phosphorylation in the presence of oxygen and through glycolysis in anaerobic environments. Vemurafenib decreases glucose uptake in sensitive human melanoma cell lines but not in intrinsically resistant lines or lines that have been passaged to become resistant. The Braf/Pten mouse model of melanoma shows no major decrease in glucose uptake with treatment with PLX4720, an analog of vemurafenib, of up to 28 days perhaps because PTEN deletion removes the negative feedback on the PI3K/mTOR pathway of cell metabolism. The decrease in uptake seen in vitro is associated with a decrease in hexokinase (HK) activity, which is required for entrapment of glucose as glucose-6-phosphate inside the cell, but not with significant changes in mRNA levels of glucose transporters or hexokinases (GLUT1, GLUT2, GLUT3, HK1, or HK2). The global effect of vemurafenib on glucose metabolism is decreased flux through glycolysis as shown by decreased lactate levels. These observations indicate vemurafenib targets the deregulated metabolism of human melanoma cells. This finding may lead to the discovery and development of novel therapeutics that specifically target the abnormal metabolism of cancer cells.

Acknowledgements

The Bosenberg Lab: Marcus Bosenberg, Katrina Meeth, Nicholas Theodosakis, Vish Muthusamy, and Manjula Santhanakrishnan.

The Office of Student Research: Dr. John Forrest, Donna Carranzo, and Mae Geter.

Howard Hughes Medical Institute

Table of Contents

INTRODUCTION

Molecular Pathogenesis and Staging of Melanoma

Melanoma is a malignancy of the pigment-producing cells of the skin called melanocytes. Two models of melanoma progression exist: one predicts melanoma formation from single cancer-prone melanocytes and another one predicts melanoma formation from malignantly transformed nevi[1]. The latter, known as the Clark model, depicts a continuous process of malignant transformation going from melanocyte to nevus with the subsequent development of dysplasia, hyperplasia, invasion, and metastasis (Figure 1).

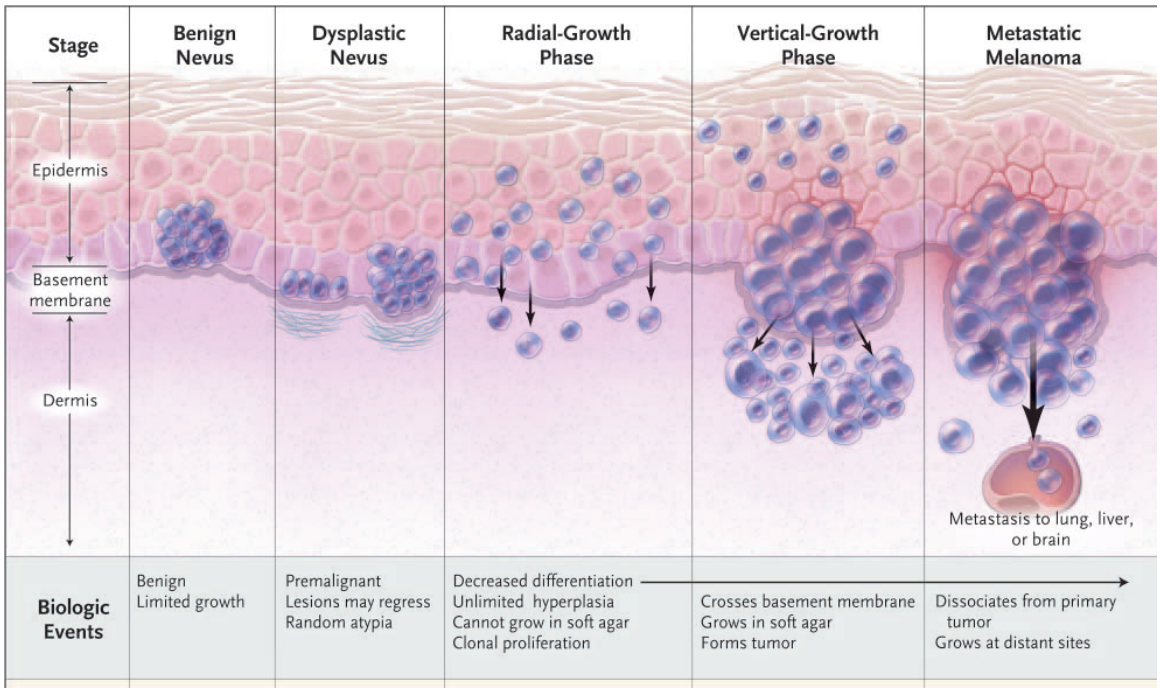

Figure 1. Biologic Events in the Progression of Melanoma. A benign nevus undergoes molecular changes that eventually lead to a premalignant dysplastic nevus, a melanoma in radial-growth phase, a melanoma in vertical-growth phase, and finally metastatic melanoma[1].

The mitogen activated protein kinase (MAP kinase) pathway is an important pathway for cell proliferation and melanomagenesis (Figure 2). It begins with a transmembrane receptor tyrosine kinase, which when bound by a growth factor, phosphorylates NRAS. Activated NRAS triggers a cascade of serine/threonine kinase phosphorylations. The main kinases of this cascade are RAF, MEK, and ERK. Once activated, ERK phosphorylates other kinases and gene regulatory proteins. By transmitting the signal downstream, activated ERK drives transcription of genes required for cell proliferation.

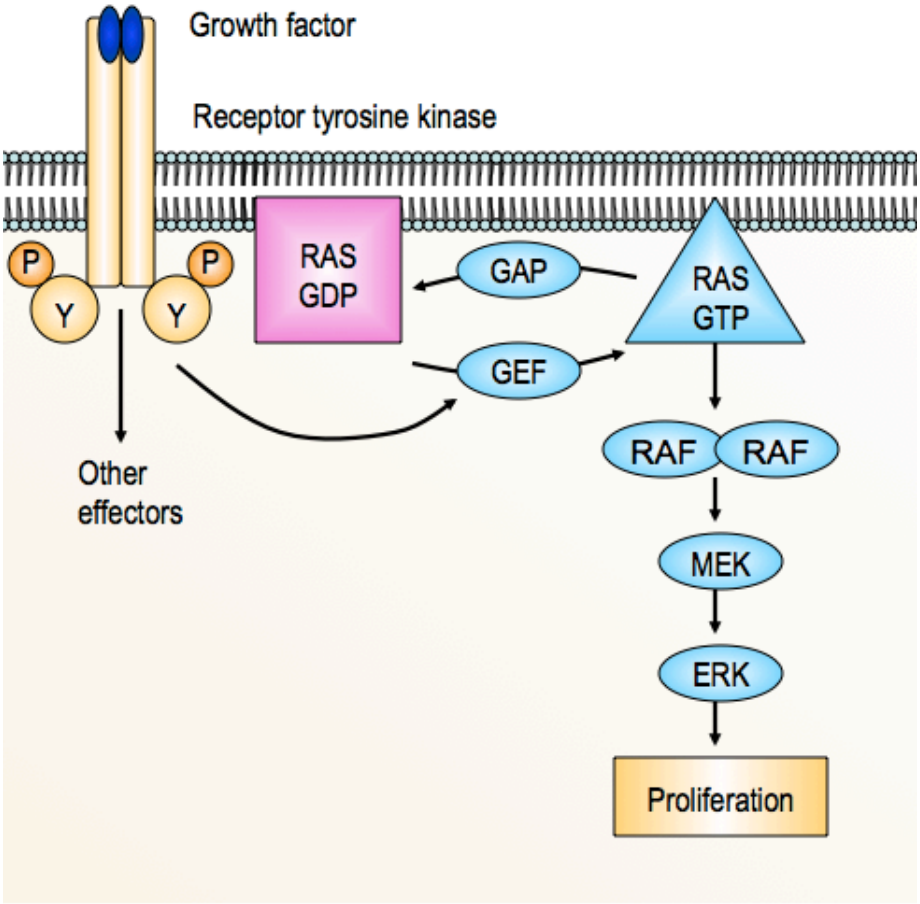

Figure 2. Mitogen Activated Protein Kinase Pathway of Cell Proliferation. Binding of growth factors to receptor tyrosine kinases on the surface of the cell activate an intracellular signaling cascade that involves RAS, RAF, MEK, and ERK.

BRAF is a serine/threonine tyrosine kinase of the MAP kinase signaling pathway of cell proliferation. This kinase plays an important role in melanocytic neoplasias[2]. *BRAF* activating mutations occur in approximately 50% of melanomas and more than 90% of these mutations result in substitution of valine for glutamic acid at the 600th amino acid (V600E)[3, 4].

Mutations in *NRAS* have been found in malignant melanoma[5-7]. A case-control study of melanoma and benign melanocytic nevi showed that 5.9% of nevi carry mutations in *NRAS*, compared to 5.2% of melanomas[8]. More recently, a systematic review of the melanoma literature revealed that the frequency of *NRAS* mutations in melanomas is much higher, at 28%[4]. Ultraviolet radiation appears to play a role in the induction of *NRAS* mutations, as most tumors carrying these genetic changes are located in areas exposed to the sun[9-11]. There is, however, conflicting evidence for the role of UV radiation in *NRAS* mutagenesis.

The mutated genes of the MAP kinase pathway, known as oncogenes because they stimulate the development of cancer, also activate counterregulatory pathways that inhibit cell proliferation in nevi, leading to growth arrest or senescence (i.e., oncogene-induced senescence, or OIS). Senescence can be caused by various stresses, including oncogene activation, telomere dysfunction, oxidative stress, DNA damage, cytotoxic drugs, and cell culture[12]. Teleologically, senescence represents an evolutionary gatekeeper against unwanted cancer formation. OIS has been shown to be an important mechanism of growth arrest in oncogenically stressed cells[13]. Loss of OIS through mutations in tumor suppressive pathways is postulated to allow oncogene-driven malignant progression of nevi to melanoma. Two main pathways have been identified:

p16INK4a-RB (retinoblastoma) and ARF-p53[14]. As expected, these two pathways are often mutated in cancer[14-17].

As part of the p16INK4a-RB pathway, the p16 (INK4) protein inhibits cell-cycle progression in response to stress by blocking the formation of an active cyclin D1-Cdk4 complex. When p16 is inactive or absent, the active cyclin D1-Cdk4 complex phosphorylates the retinoblastoma protein (Rb), rendering it nonfunctional. Phosphorylated Rb releases the gene regulatory protein E2F, allowing expression of S-phase genes and progression of the cell cycle even in the context of damaging environmental or intrinsic stressors.

The tumor suppressor protein p53 is mutated in about half of all human cancers, making it a paramount gene in human cancer. The protein is involved in cell cycle control, apoptosis, and maintenance of genetic stability. Oncogene-driven cell proliferation stimulates the ARF protein, which then activates p53. DNA damage may also stimulate p53 activation. Activated p53 induces the cell to commit suicide by apoptosis or blocks cell division until the damage is repaired. The p53 protein inhibits cell cycle progression by binding to DNA and inducing transcription of the *CDKN1A* (*p21*) gene. The p21 protein binds to Cdk complexes, preventing the cell from entering S-phase and replicating its DNA.

Tissue markers for senescence include senescence-associated β-galactosidase (SA-β-Gal), p16, p53, and p21. Staining of cells or tissue sections with the chromogenic substrates X-gal or fluorescein di-β-d-galactopyranoside (FDG) for the detection of SA-β-Gal activity is the most widely used assay for the detection of OIS. Enzymatic activity is derived from the increased lysosomal content of senescent cells; its biological

significance, however, is still uncertain. Levels of p16, p53, and p21 can be measured by means of immunohistochemistry and Western blotting.

Several studies of melanocytic neoplasia provide evidence that OIS is partly responsible for the growth-arrested state of nevi and that loss of senescence-inducing signaling pathways is associated with progression to melanoma. Normal human melanocytes transduced with the oncogene $BRAF^{V600E}$ show early growth followed by arrest after 21 days of culture[18]. Growth arrest correlated with SA-β-galactosidase activity and elevated levels of p16. Human melanocytic nevi, irrespective of *BRAF* mutational status, also display these markers and lack staining for the proliferation marker Ki-67 on immunohistochemistry. These findings are consistent with the OIS hypothesis of nevi.

Immunohistochemical comparison of benign compound nevi, dysplastic nevi, and melanomas has also shed light on the role of the senescence-inducing pathways (e.g. p16INK4a-RB and ARF-p53) in melanoma development and progression[19]. Benign compound nevi show SA-β-galactosidase reactivity and intense p16 nuclear staining, whereas p53 and p21 are not detectable. Dysplastic nevi, in contrast, showed less extensive staining for p16 than benign compound nevi. Furthermore, staining was limited to the cytoplasm, a pattern that is associated with dysfunctional p16. A proportion of nevi showed pockets of p53-positive cells, often without p21, suggesting that benign nevi are in a p16-dependent senescent state whereas dysplastic areas of nevi may still be proliferating. Supporting this hypothesis, nevi from patients with a mutation that inhibits nuclear translocation of p16, an event required for fully functional p16, tend to be large

and of atypical appearance[20]. Furthermore, the tumor suppressors p21 and p53 are expressed widely in these nevi.

Melanomas showed a few areas of immunoreactivity to p21 and p53, typically at the edges of the lesion, with the bulk of the nodule being negative. Likewise, most areas lacked detectable levels of p16, a finding more common in vertical growth-phase (VGP) melanomas compared to radial growth-phase (RGP) melanomas. Although the staining pattern of p21, p53, and p16 was similar between dysplastic nevi and the edges of melanomas, the latter showed more intense reaction to CHK2, a checkpoint kinase that mediates p53 activation on DNA damage and p53-dependent senescence. The edges of melanomas may represent residual senescent regions, namely nevi.

A study using a mouse model of melanoma showed that p16 might play a less prominent role in OIS than originally thought[21]. Mice harboring the $BRAF^{V600E}$ mutation developed nevi regardless of the mutational status of *CDKN2A (p16)*. This means that nevi in *CDKN2A*-null mice entered senescence through an alternative tumor suppressive pathway. Furthermore, tumors in mice carrying wild-type *CDKN2A* retained nuclear expression of p16, suggesting that, in contradiction with other studies, disruption of the p16INK4a-RB pathway is not necessary for melanoma progression. However, the study showed that *CDKN2A*-null mice were more likely to develop melanomas than wild-type *CDKN2A* mice (80% vs. 54% at 12 months). In addition, melanomas developed earlier in the *CDKN2A*-null mice than in the wild type mice (50% of mice developed tumors at 7 months vs. 12 months). Finally, tumors in the *CDKN2A*-null mice were multiple whereas the wild type mice developed single tumors. These results suggest p16 increases tumor penetrance and decreases latency.

A biopsy of clinically suspicious lesions, which are those showing asymmetry, irregular borders, variation in color, diameter of greater than 6mm, and recent evolution in appearance (ABCDE criteria), provides histologic confirmation of cutaneous melanoma[22]. According to the American Joint Committee on Cancer, staging of melanoma is based on maximal thickness of the tumor (T), presence or absence of microscopic ulceration, the number and size of involved lymph nodes (N), and the presence or absence of metastasis (M) (Tables 1 and 2)[23].

Table 1. TNM Staging Categories for Cutaneous Melanoma

Classification	Thickness (mm)	Ulceration Status/Mitoses
T		
Tis	NA	NA
T1	≤ 1.00	a: Without ulceration and mitosis < 1/mm^2 b: With ulceration or mitoses ≥ 1/mm^2
T2	1.01-2.00	a: Without ulceration b: With ulceration
T3	2.01-4.00	a: Without ulceration b: With ulceration
T4	> 4.00	a: Without ulceration b: With ulceration
N	**No. of Metastatic Nodes**	**Nodal Metastatic Burden**
N0	0	NA
N1	1	a: Micrometastasis* b: Macrometastasis†
N2	2-3	a: Micrometastasis* b: Macrometastasis† c: In transit metastases/satellites without metastatic nodes
N3	4+ metastatic nodes, or matted nodes, or in transit metastases/satellites with metastatic nodes	
M	**Site**	**Serum LDH**
M0	No distant metastases	NA
M1a	Distant skin, subcutaneous, or nodal metastases	Normal
M1b	Lung metastases	Normal
M1c	All other visceral metastases	Normal
	Any distant metastasis	Elevated

Abbreviations: NA, not applicable; LDH, lactate dehydrogenase.
*Micrometastases are diagnosed after sentinel lymph node biopsy.
†Macrometastases are defined as clinically detectable nodal metastases confirmed pathologically.

Table 2. Anatomic Stage Groupings for Cutaneous Melanoma

	Clinical Staging*				Pathologic Staging†		
	T	N	M		T	N	M
0	Tis	N0	M0	0	Tis	N0	M0
IA	T1a	N0	M0	IA	T1a	N0	M0
IB	T1b	N0	M0	IB	T1b	N0	M0
	T2a	N0	M0		T2a	N0	M0
IIA	T2b	N0	M0	IIA	T2b	N0	M0
	T3a	N0	M0		T3a	N0	M0
IIB	T3b	N0	M0	IIB	T3b	N0	M0
	T4a	N0	M0		T4a	N0	M0
IIC	T4b	N0	M0	IIC	T4b	N0	M0
III	Any T	N > N0	M0	IIIA	T1-4a	N1a	M0
					T1-4a	N2a	M0
				IIIB	T1-4b	N1a	M0
					T1-4b	N2a	M0
					T1-4a	N1b	M0
					T1-4a	N2b	M0
					T1-4a	N2c	M0
				IIIC	T1-4b	N1b	M0
					T1-4b	N2b	M0
					T1-4b	N2c	M0
					Any T	N3	M0
IV	Any T	Any N	M1	IV	Any T	Any N	M1

*Clinical staging includes microstaging of the primary melanoma and clinical/radiologic evaluation for metastases. By convention, it should be used after complete excision of the primary melanoma with clinical assessment for regional and distant metastases.

†Pathologic staging includes microstaging of the primary melanoma and pathologic information about the regional lymph nodes after partial (ie, sentinel node biopsy) or complete lymphadenectomy. Pathologic stage 0 or stage IA patients are the exception; they do not require pathologic evaluation of their lymph nodes.

Treatments of Metastatic Melanoma

One American dies from melanoma almost every hour [24]. Patients with metastatic disease have a poor prognosis, with a median survival of <1 year [23]. Durable responses are achieved in <10% of patients with metastatic melanoma treated with high-dose interleukin-2 [25]. Ipilimumab (CTLA4 blocking antibody) has shown a survival benefit in patients with metastatic melanoma, but long-term benefit was observed for only an additional 10% of patients compared with control arm therapy in randomized, phase III trials [26, 27]. New treatments are needed.

The increased knowledge about the molecular pathogenesis of melanoma has opened the door to a personalized approach to the treatment of melanoma. BRAF mutations have been found in ~50% of melanomas, and most of these mutations result in a substitution of glutamic acid for valine at the 600th amino acid of the BRAF protein chain (V600E) [3]. BRAF is a kinase that is part of the BRAF→MEK→ERK mitogen-activated protein kinase (MAPK) pathway of cell proliferation. The mutated kinase is constitutively active and, in combination with other molecular oncogenic changes, results in unregulated cell proliferation. In clinical trials, the selective BRAF inhibitor vemurafenib (formerly known as PLX4032, RG7204, and RO5185426) produced complete or partial tumor regression in most patients [28]

Despite the promising results of these trials and the demonstrated clinical benefit, responses are short-lived in many patients as a result of mechanisms that are not fully understood. Some studies have shed light on the molecular correlations of drug resistance (Figure 3). Melanoma cell lines treated with BRAF inhibitors show rebound phosphorylated ERK (pERK) activation and escape from BRAF inhibition [29]. Second-site mutations that confer resistance have not been observed in BRAF to date [30]. It is crucial to gain a thorough understanding of the underlying mechanisms so that we can develop novel strategies to circumvent resistance and achieve more prolonged responses.

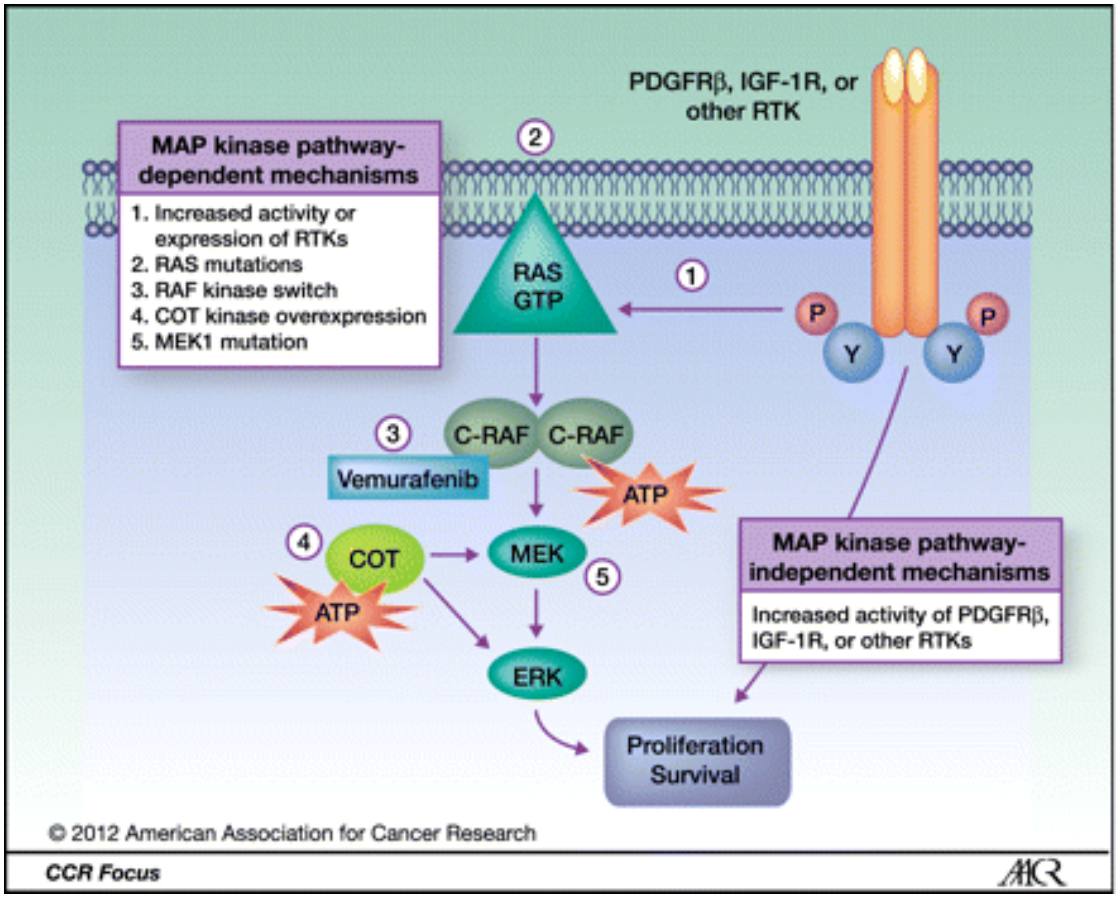

Figure 3. Mechanisms of Resitance to Vemurafenib. Various mechanisms of resistance have been elucidated. Some depend on the MAP kinase pathway while others work independently of this pathway.

Clinical trials for vemurafenib

The current treatments for metastatic melanoma (i.e., interleukin-2 and dacarbazine) are largely ineffective because they provide no improvement in overall survival [31]. Dacarbazine in particular has a response rate of only 15% to 20%. The discovery that >50% of melanomas harbor a mutation in the *BRAF* gene heralded the development of targeted therapies against the corresponding mutant, activated protein [3].

The small-molecule BRAF inhibitor vemurafenib showed promising results in a phase I trial [28]. This multicenter phase I trial consisted of 2 phases: a dose-escalation phase and an extension phase. In the dose-escalation phase, investigators determined the

recommended extension phase and phase II dose to be 960 mg twice daily. Higher doses than this resulted in intolerable fatigue, rash, and arthralgias. Another common adverse event was squamous cell carcinoma, keratoacanthoma-type. These well-differentiated skin tumors have low invasive potential and no metastatic potential, and they can be easily excised. The purpose of the extension phase was to determine the response rate according to Response Evaluation Criteria in Solid Tumors (RECIST) in patients with metastatic melanoma harboring the *BRAF* V600E mutation. Patients with brain metastases were excluded from the study. Of the 32 patients in the extension cohort, 26 (81%) responded to treatment, with 68% of all patients having responses that were sufficiently durable to be confirmed on subsequent scans. Two patients showed a complete response, and 24 showed partial responses. Although some responses are transient, with a median progression-free survival (PFS) time of ~7 months (including both responders and nonresponders), some patients show continued response for >2 years [32].

The single-arm, multicenter, open-label phase II trial known as BRIM2 had a primary endpoint of overall response rate, with a target of 20%, and secondary endpoints of duration of response, PFS, and overall survival [32]. A total of 132 previously treated patients with $BRAF^{V600E}$-positive metastatic melanoma were enrolled in the study. A companion diagnostic assay co-developed with vemurafenib, known as the cobas 4800 *BRAF* V600E Mutation Test (Roche Molecular Diagnostics), was used to determine the BRAF mutational status of patients enrolled in the study. All patients were treated with 960 mg of vemurafenib twice daily until disease progression occurred. At the time of analysis, the median follow-up was 7 months. With a response rate of 52% (62/132),

consisting of 59 partial responses and 3 complete responses, the trial met its primary endpoint. The median duration of response was 6.8 months, and the median PFS was 6.2 months. Consistent with the phase I trial, the most common side effects (>25%) were rash, fatigue, and arthralgias. The most common grade 3 adverse event was cutaneous squamous cell carcinoma (24.2%), which was excised without interfering with the trial.

An additional study was conducted to investigate whether vemurafenib is associated with improved survival compared with dacarbazine, the standard of care. This study, a global, randomized, open-label, controlled, multicenter phase III trial known as BRIM3, accrued 675 untreated patients with $BRAF^{V600E}$-positive metastatic melanoma [33]. The study met the primary endpoints of showing improvement in overall survival and PFS at the time of the interim analysis, which occurred 1 month after the last patient was accrued. With a median follow-up of just over 3 months, the interim analysis revealed that the vemurafenib group achieved a 6-month overall survival of 84%, compared with 64% in the dacarbazine group. On the basis of these extraordinary results, patients in the dacarbazine group were allowed to switch immediately to the vemurafenib group. The median PFS was 5.3 months for vemurafenib compared with 1.6 months for dacarbazine. Consistent with previous trials, the response rate of vemurafenib was 48% compared with 5% for dacarbazine, and the grade 3 or worse adverse effects consisted primarily of arthralgias (3%), rash (8%), fatigue (2%), and cutaneous squamous cell carcinomas or keratoacanthoma (20%).

Vemurafenib is the first personalized treatment for metastatic melanoma to show an improvement in overall survival, and it was approved by the U.S. Food and Drug

Administration in 2011.

Metabolism and Cancer

Cancer is characterized by uncontrolled cell proliferation. Recently, deregulated metabolism has been identified as an emerging hallmark of cancer[34]. Alterations in energy metabolism are necessary to fuel the rapid cell growth and division of malignant cells. Normal cells utilize glucose in two different ways depending on the availability of oxygen. In the presence of oxygen, normal cells metabolize glucose through glycolysis to pyruvate in the cytosol and then shunt it to the mitochondria for oxidative phosphorylation. In the absence of oxygen, normal cells break down glucose to lactate via glycolysis and fermentation. Cancer cells, in contrast, partially reprogram their metabolism to increase conversion of pyruvate to lactate irrespective of oxygen availability. The metabolism of glucose through glycolysis with the production of lactate is known as aerobic glycolysis.

To allow for increased lactate production and the maintenance of ATP synthesis, cancer cells markedly upregulate glucose uptake, in part by increasing expression of glucose transporters, such as GLUT1[35-37]. This observation forms the basis for visualizing glucose uptake using positron emission tomography (PET) with a radiolabeled analog of glucose, specifically ^{18}F-fluorodeoxyglucose, as a reporter. Another glucose analog that is used to study glucose metabolism is the fluorescence analog called 2-[*N-(*7-nitrobenz-2-oxa-1,3-diazol-4-yl)amino]-2-deoxyglucose (2-NBDG) [38]. This analog is phosphorylated by hexokinases but is not further metabolized.

Increased glycolysis, while generating less ATP per glucose molecule than oxidative phosphorylation, allows for the production of metabolic intermediates for various biosynthetic pathways, including those of amino acids and nucleosides. The result is an increased availability of building blocks for proteins and nucleic acids to assemble organelles and form new cells.

The PI3K-mTOR pathway is an important pathway for metabolism, both in normal and cancer cells. For this reason, multiple clinical trials of agents that target the pathway are currently ongoing[39]. Activation of the pathway can involve binding of insulin-like growth factors (IGFs) to IGF receptors. This event activates phosphoinositide 3-kinase (PI3K), which after a number of steps leads to activation of the mammalian target of rapamycin (mTOR). The tumor suppressor PTEN negatively regulates PI3K activation. The mTOR protein plays a central role in cell metabolism by regulating protein translation (Figure 4).

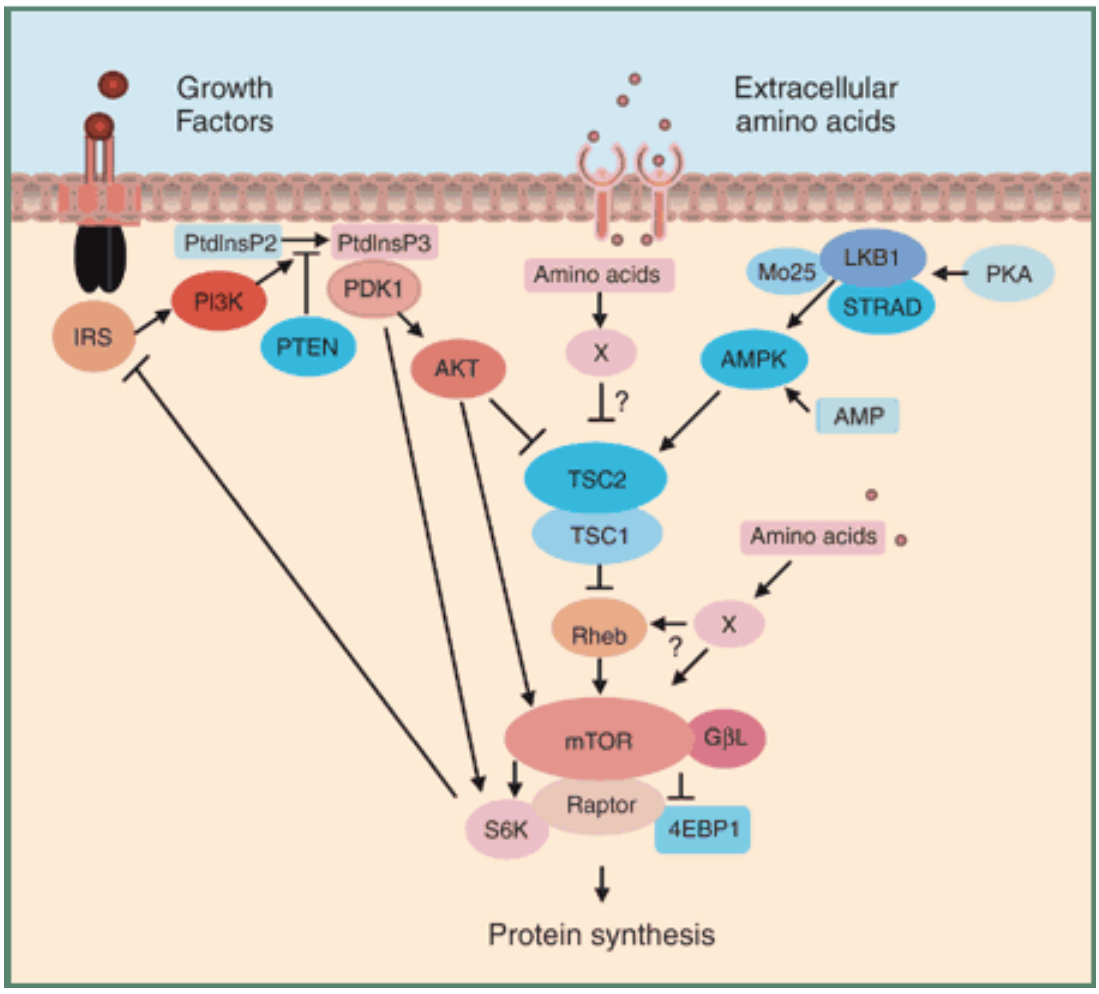

Figure 4. PI3K-mTOR pathway. Binding of insulin-like growth factors to membrane receptors leads to activation of the PI3 kinase, leading to conversion of PI2P into PI3P. PI3P activates PDK1, which phosphorylates AKT. AKT activates mTOR, promoting protein synthesis[40].

Cell metabolism may play an important role in measuring responses to targeted cancer therapies. A study that evaluated FDG-PET responses to vemurafenib in BRAF-mutant advanced melanoma showed a trend for patients with greater reductions in uptake of FDG to have longer progression-free survival[41]. At the same time, there was no relationship between best response according to RECIST criteria and progression-free survival.

STATEMENT OF PURPOSE: SPECIFIC HYPOTHESIS AND SPECIFIC AIMS OF THE THESIS

Hypothesis: vemurafenib targets the deregulated metabolism of cancer cells.

Aims:

- Evaluate glucose uptake in human melanoma cell lines *in vitro*.
- Evaluate glucose uptake in the *Braf/Pten* mouse model.
- Characterize the mechanism of decreased glucose uptake.
- Evaluate the global metabolic effect of treatment with vemurafenib.

METHODS

In vitro Glucose Uptake Assay*

Cells from the lines 501Mel, YUKSI, YUKOLI, YURIF, YUCOT, YULAC-sensitive, and YULAC-resistant were cultured overnight in 2mL of Opti-MEM supplemented with 10% FBS at 37°C and 5% CO_2 in six-well plates at a density of 50,000 cells/mL. The YULAC-resistant line was generated by passaging the YULAC-sensitive line in medium containing 1 μM PLX4032 for several months. Each plate corresponded to a specific time point. After overnight incubation, three wells were treated with 3 μM PLX4032 (vemurafenib) and the other three wells were treated with control vehicle of DMSO. For some cell lines, experiments were also performed with cells treated with 300 nM MEK inhibitor and high concentrations of PLX4032 and MEK inhibitor. At time 0, after treatment, cells were washed gently with PBS. Then they were incubated in 150 μL of 300 μM 2-NBDG (Invitrogen) for 10 minutes and washed gently three times with cold PBS. Next, they were visualized with a fluorescence microscope equipped with a FITC filter and the intensity of the 2-NBDG signal was subjectively scored using a scale from 0 (no signal, i.e. control wells) to 3 (maximum intensity). The above steps were repeated for time points 7 hours, 9 hours, 12 hours, 24 hours, 48 hours, and 72 hours.

Duplicate plates were made to measure the viability of the cells to ensure changes in uptake were not due to cell death. Cell viability was measured by automatic trypan

---

* **Development and optimization of method as well as experiments on lines YULAC-sensitive and –resistant performed by author; other cell lines evaluated by Nicholas Theodosakis.**

blue assay (Cell Countess).

Glucose Uptake In Vivo*

The Braf/Pten mouse model is an immunocompetent mouse model that relies on the Cre-Lox recombination system[42]. Briefly, the Cre recombinant enzyme gene is fused to an estrogen receptor gene. Expression of this construct is under control of the tyrosinase promoter, ensuring expression is limited to melanocytes. The Cre-ER fusion protein is inactive until 1 µL of 50 mg/mL 4-hydroxytamoxifen diluted six-fold in 100% ethanol is applied to the skin of the mouse. The 4-hydroxytamoxifen binds to the estrogen receptor and activates the Cre recombinase. Next, the Cre-ER enzyme recombines DNA between loxP sites. Through this mechanism $Braf^{WT}$ transforms into $Braf^{V600E}$ and Pten is deleted. Two weeks after induction a melanoma tumor begins to be visible at the site of 4-hydroxytamoxifen application.

Mice underwent melanoma induction this way and then were treated starting at week 2 after induction with an analog of vemurafenib, PLX4720, for 0, 7, 14, 21, and 28 days. The PLX4720 was compounded in mouse chow to yield a dose similar to what is achieved in human patients . At the given time points, the mouse was injected with 100 µL of 700 µM 2-NBDG retro-orbitally. Analogous to the use of ^{18}F-fluorodeoxyglucose for imaging of tumors using a PET scanner, the mouse was imaged using the Maestro in vivo imaging system (CRI) and the Maestro imaging software for detection of glucose uptake in the tumor 30 minutes after injection of 2-NBDG to allow distribution of the 2-NBDG throughout the mouse's body and tumor. The mouse was anesthetized in an

* Performed by author

isoflurane chamber for injection of 2-NBDG and imaging. The images were acquired and analyzed as outlined in the system's instructions manual.

Quantitative RT-PCR[*]

The cDNA levels of GLUT1, GLUT3, HK1, HK2, and HK3 in YULAC (sensitive) both under treatment with 3 μM PLX4032 (vemurafenib) and control were measured by quantitative RT-PCR using the TaqMan® Gene Expression Assay and the StepOne™ Real-Time PCR System.

Hexokinase Assay[†]

The hexokinase assay (Biomedical Research Service Center University at Buffalo, State University of New York, Cat #: E-111) was performed by following the protocol previously described. Briefly, cell lysis solution was added to 10^5-10^6 pelleted cells of the cell lines YULAC-sensitive and 501Mel. The cell lines were incubated in 3 μM PLX4032 or DMSO control for 3 days. Lysate was centrifuged and supernatant was recovered for HK assay. Bradford protein assay was performed to determine sample protein concentrations for normalization. The sample protein concentration was normalized to 0.2-1 mg/mL by diluting in ice-cold cell lysis solution. Next, 10 μL of sample for each cell line was added in triplicate to a 96-well microplate. The reaction was initiated by adding 50 μL of working HK assay solution to each well. The plate was covered and incubated at 37°C for 30 minutes. Subsequently, the reaction was stopped by adding 50 μL of 3% acetic acid per well. Optical density was measured at 492 nm using a

[*] Performed by author.
[†] Performed by Nicholas Theodosakis

microplate reader and compared between experimental conditions and cell lines by using a two-tailed Student's T-test.

Tritiated 3-O-Methylglucose Uptake Assay*

The purpose of this assay is to determine whether treatment with vemurafenib decreases glucose uptake by affecting the function of the glucose transporter (by means of translocation or inactivation) or by affecting the function of hexokinase (by downregulation of expression or inactivation). The protocol was modified from the literature [43,44,45].

Cells were seeded in 6-well plates at predetermined cell densities, 2 mL/well and incubated for 1 day at 37°C, 5% CO_2. Then they were incubated in 3 μM vemurafenib (3 wells) or vehicle (3 wells) for 72 hours. Duplicate plates were generated for cell counting since control vs. treated wells have different cell densities at 72 hours. At 72 hours, cells were washed with 1 mL PBS followed by the addition of 1 mL of PBS. Next, 10 μL of tritiated 3-O-methylglucose stock solution (100X) were added and the plates were incubated for 30 seconds, 60 seconds, and 3 minutes.

The 3-O-methylglucose stock solution was prepared as follows. A volume of 50 uL of [^{3}H]3-O-methylglucose (American Radiolabeled Chemicals, cat. No. NET379001MC, 60-90 Ci/mmol, 1 mCi/ml in ethanol-water 9:1) was added to 450 μL of 1 g/L 3-O-methylglucose (3-O-methyl-D-glucopyranose; Sigma-Aldrich, cat. No. 101176252, 1 g – FW 194.18 g/mol) in PBS with Ca/Mg to make a 100X, 100 μCi/mL, 5 mM 3-O-methylglucose stock solution.

At the end of each time point, cells were washed three times with 500 μL ice-cold

* Performed by author

PBS supplemented with 100 μM phloretin. Phloretin is a compound that blocks glucose transporters and ensures the level of radioactivity measured from the samples comes from the intracellular stores of tritiated 3-O-methylglucose. Next, 300 μL of modified RIPA buffer was added for cell lysis and the plate was incubated for 10 min. The entire cell lysate was transferred into a scintillation vial containing 3 mL of liquid scintillation cocktail (ICN). To collect any remaining lysate, 300 μL PBS buffer was added into each well for washing and then this buffer was transferred into the corresponding scintillation vial. A second wash and collection of buffer was performed followed by vortexing of the scintillation vial (total 3.9 mL) for a few seconds.

The radioactivity associated with the cells was quantified using a scintillation counter (the "counts per minute or cpm of each scintillation vial). A volume consisting of 600 μL PBS, 300 μL modified RIPA buffer, and 3 mL of scintillation fluid served as a blank and 10 μL of 3-O-MG stock solution served as the external standard.

Metabolic Flux Cell Labeling*

Melanoma cells were labeled with ^{13}C-glucose and – glutamine as previously described[46].

Briefly, melanoma cells were seeded into 6-well plates such that at the end of the labeling period they were at confluency (plated 2 mL at density of ~75,000 cells/mL in Opti-MEM with 10% v/v FBS, 1% v/v pen/strep and supplemented with 3 μM PLX4032 in treated wells and DMSO in control wells). For each condition, cells were seeded into 4 wells (3 for gas chromatography-mass spectroscopy analysis, 1 for protein determination). After 24 hours to allow cell to attach to plate and following incubation

* **Performed by author**

for two days, 1 mL of medium was saved. The sample was centrifuged to remove floating cells and the supernatant was collected and then shipped. Next, the growth medium was replaced with 2mL/well of glucose labeling medium (MEM--Cellgro 15-010: 1 g/L glucose, no glutamine--supplemented with 1 g/L [U-^{13}C6] glucose, 10% v/v FBS, 1mM L-glutamine, 1% v/v pen/strep, 1% v/v MEM vitamins, 1X NEAA) or 2mL/well of glutamine labeling medium (MEM--Cellgro 15-010: 1 g/L glucose, no glutamine--supplemented with 1 g/L unlabeled glucose, 10% v/v FBS, 0.5 mM unlabeled L-glutamine, 0.5 mM [U-^{13}C5] L-glutamine, 1% v/v pen/strep, 1% v/v MEM vitamins, 1X NEAA). Medium to be added to treated cells was supplemented with 3 μM PLX4032. Cells were incubated in the labeling media for 8 hours and 24 hours.

For extraction, 1mL of medium from labeled cells was saved. Floating cells were removed by centrifugation and the supernatant was collected and shipped. Cells were collected by trypsinization and spun down at 500 x g at 4°C. Cells were kept on ice after they were harvested. Cells were resuspended in 1mL of ice-cold PBS and transferred into Eppendorf tubes. Then they were spun down at 500 x g for 5 minutes and the PBS was removed without disturbing the cell pellet. The cells were placed on dry ice for freeze down. The frozen pellets were kept at -70°C. The frozen samples were then shipped on dry ice overnight.

Shipments were sent to Sanford-Burnham at University of California-San Diego for gas chromatography-mass spectrometry analysis (GC-MS) following a previously described protocol[46].

RESULTS

2-NBDG in vitro uptake assay:

To evaluate the effect of vemurafenib treatment on glucose uptake melanoma cells were exposed to the glucose analog 2-NBDG in vitro. The most sensitive cell line to PLX4032, YULAC-sensitive, showed a gradual decrease in glucose uptake, starting at a time between 7 and 9 hours. Uptake decreased to undetectable levels at 48 hours. In contrast, the resistant counterpart showed no decrease in uptake (Figure 5). YUCOT, another sensitive line showed decreased uptake as early as 9 hours after incubation in PLX4032 (Figure 6). The moderately sensitive lines YUKOLI and YURIF showed minor decrease in uptake at 72 and 24 hours, respectively. The resistant line YUKSI showed no decrease in uptake while the other resistant line 501Mel showed a minor decrease in uptake as early as 7 hours.

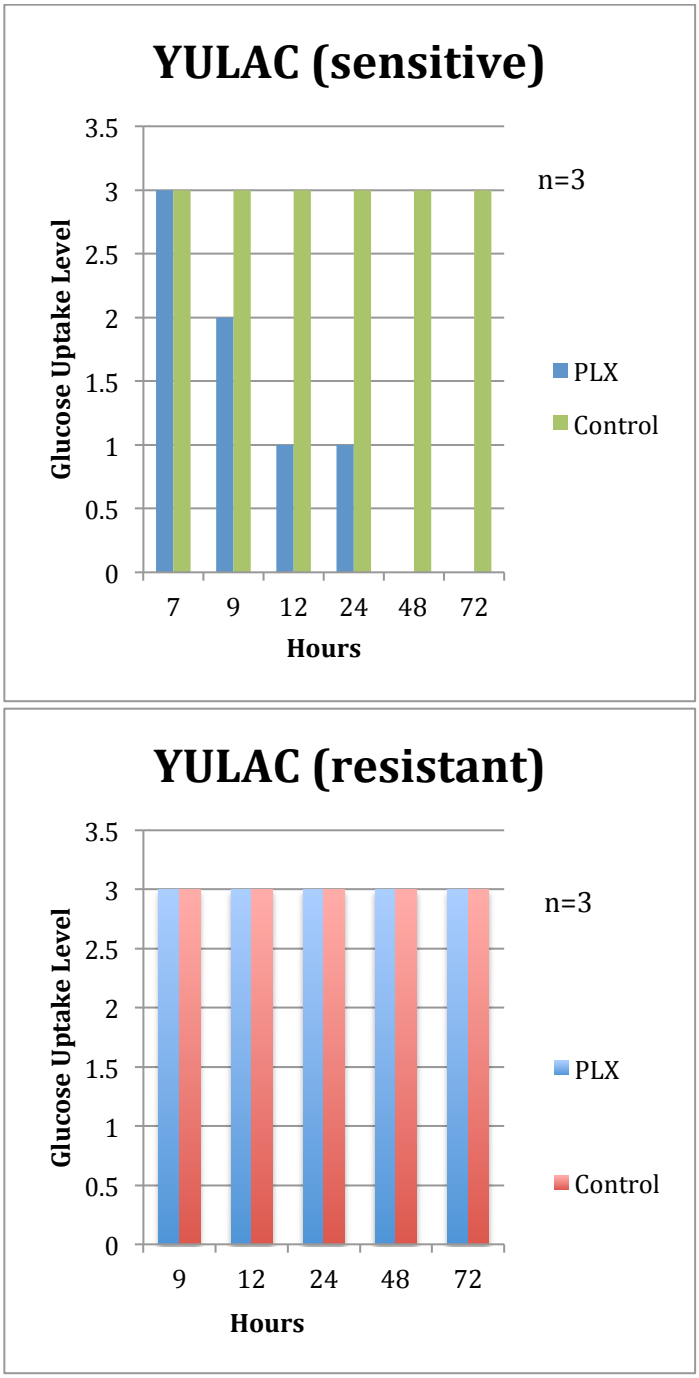

Figure 5. Effect of PLX4032 on glucose uptake in human melanoma cell lines YULAC-sensitive and -resistant. YULAC-sensitive is susceptible to the inhibitory effect of PLX4032 on glucose uptake. In contrast, acquired resistance YULAC is not.

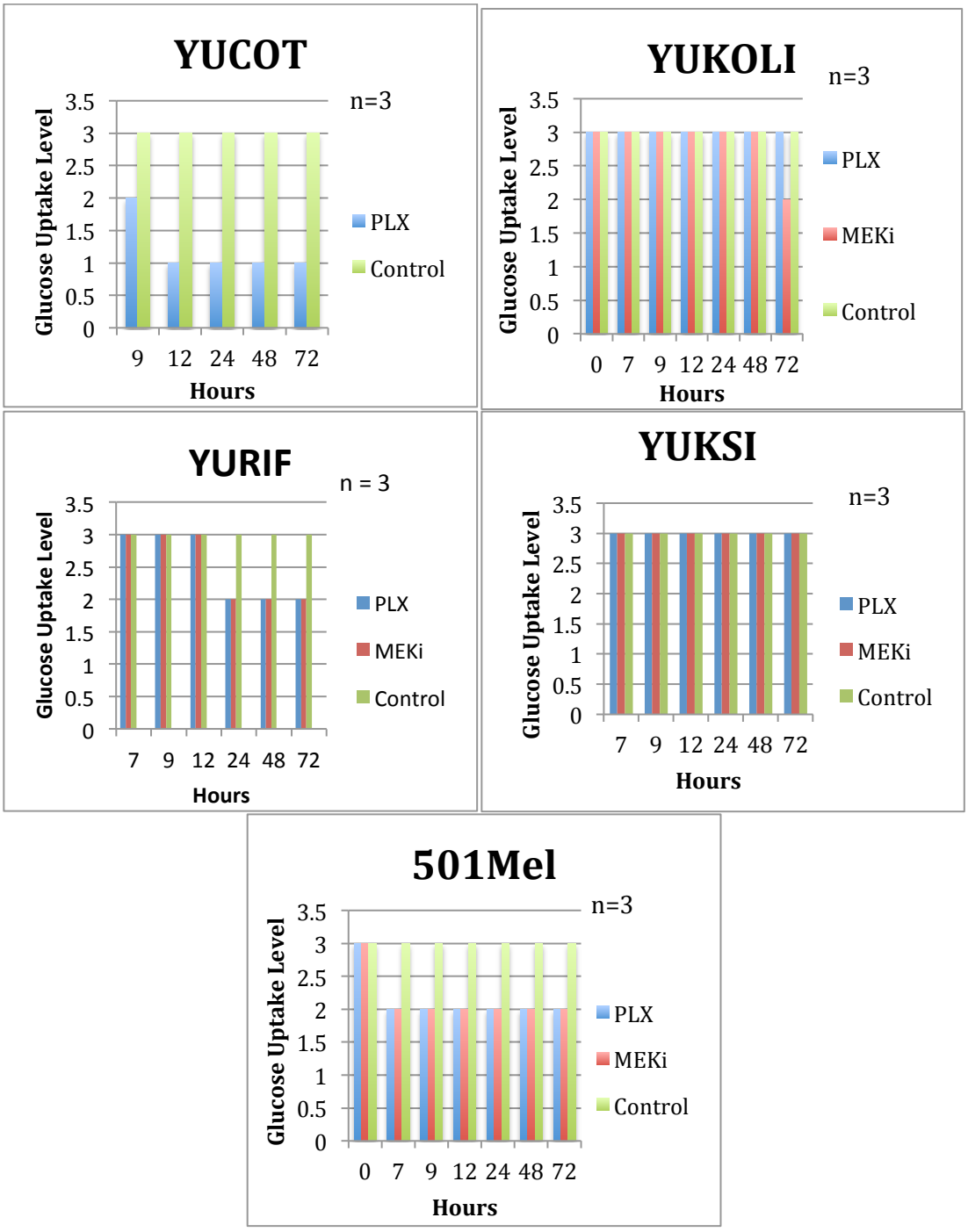

Figure 6. Effect of PLX4032 on glucose uptake in the human melanoma cell lines YUCOT, YUKOLI, YURIF, YUKSI, and 501Mel.

In vivo glucose uptake assay

To evaluate the effect of treatment with vemurafenib on glucose uptake in melanoma cells in vivo, a Braf/Pten mouse bearing a melanoma tumor was treated with the vemurafenib analog, PLX4720, and imaged using the glucose analog 2-NBDG. No definitive decrease in glucose uptake was observed in the melanoma tumor at 0, 7, 14, 21, or 28 days after initiation of treatment with PLX4720 (Figure 7).

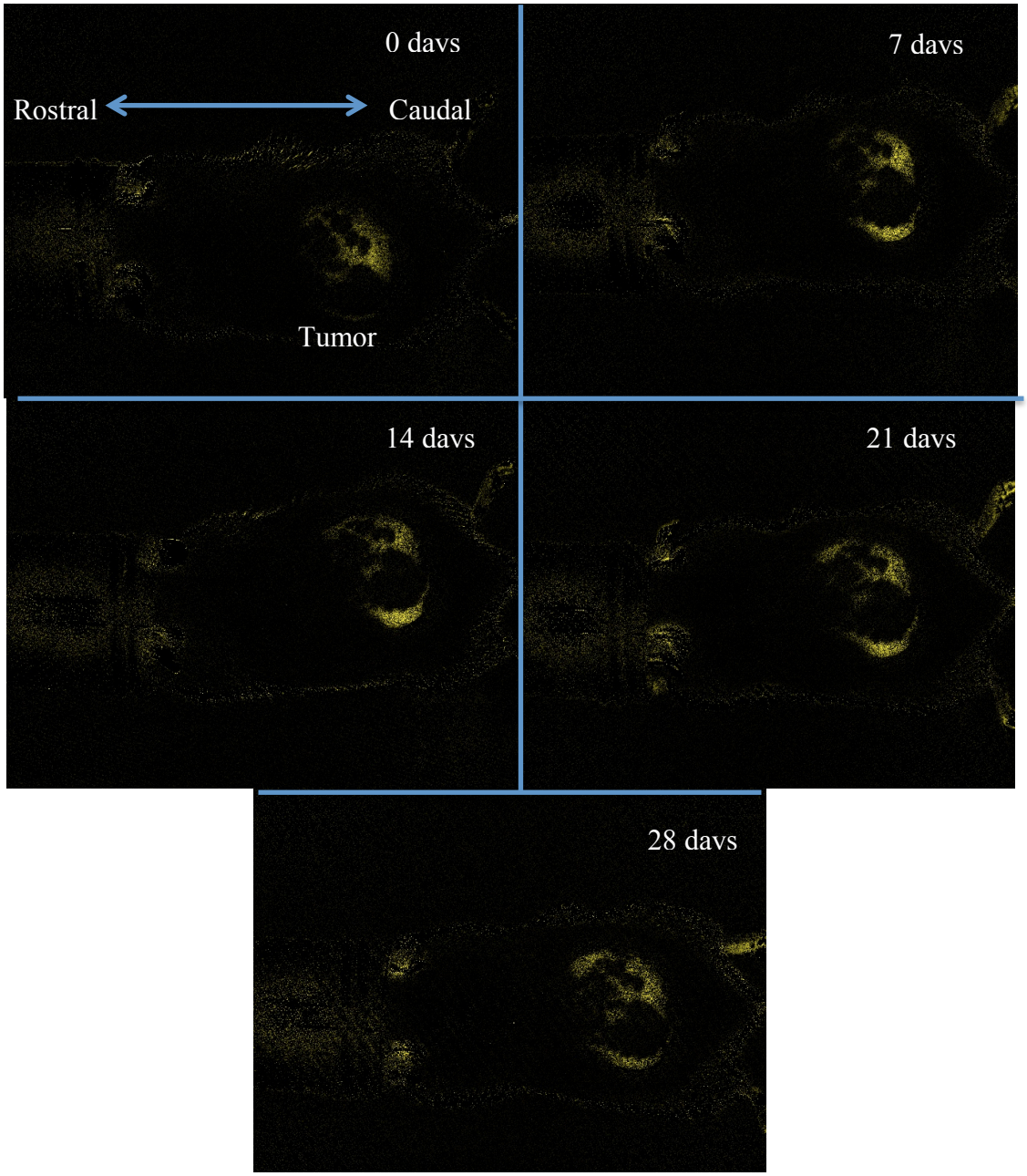

Figure 7. Effect of the vemurafenib analog, PLX4720, on glucose uptake in the Braf/Pten mouse melanoma model. No effect on glucose uptake was observed up to 28 days of treatment.

qRT-PCR levels

Given the delayed time-course of decrease in glucose uptake observed in vitro, it was possible that vemurafenib decreased glucose uptake by inhibiting the transcription of the genes required for glucose uptake, namely the glucose transporters and the

hexokinases. To test this possibility quantitative RT-PCR was performed. The change in mRNA levels of glucose transporter genes was not significant (data not shown). .

HK activity assay

Hexokinase phosphorylates glucose that enters the cell and converts it into glucose-6-phosphate, a form that is trapped intracellularly. To investigate whether vemurafenib decreases glucose uptake in melanoma cell lines by altering the function of hexokinase, a hexokinase activity assay was performed. The hexokinase activity level was halved in the YULAC-sensitive cell line ($p<0.05$) whereas no change was observed in the most resistant line, 501Mel (Figure 8). The assay neither distinguishes among the three hexokinases (HK1, HK2, and HK3) nor gives an indication as to the alteration that results in the drop in activity level.

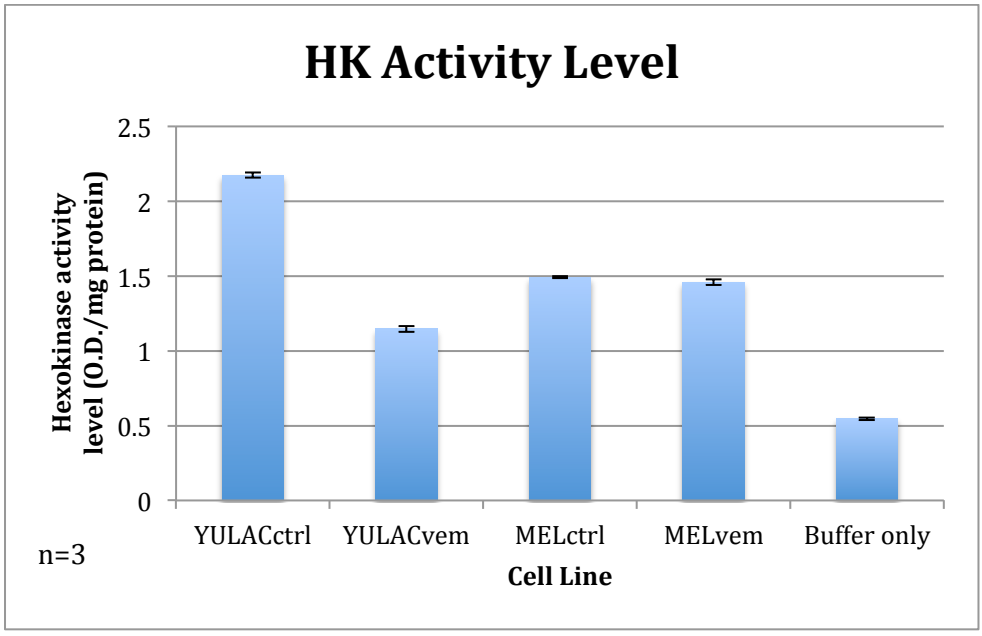

Figure 8. Effect of treatment with vemurafenib on hexokinase activity level in the YULAC-sensitive and 501Mel (resistant) human melanoma cell lines.

3-O-Methylglucose Uptake Assay

To evaluate whether vemurafenib treatment decreases the number of glucose transporters, a time-course of tritiated 3-O-methylglucose uptake was generated. Hexokinase cannot phosphorylate this glucose analog. The uptake of 3-O-methylglucose showed no difference between the control and treated samples in the YULAC-sensitive line. In contrast, 501Mel showed increased uptake with treatment at 30 and 60 seconds ($p<0.05$) (Figure 9). The mechanism for this increase is unclear.

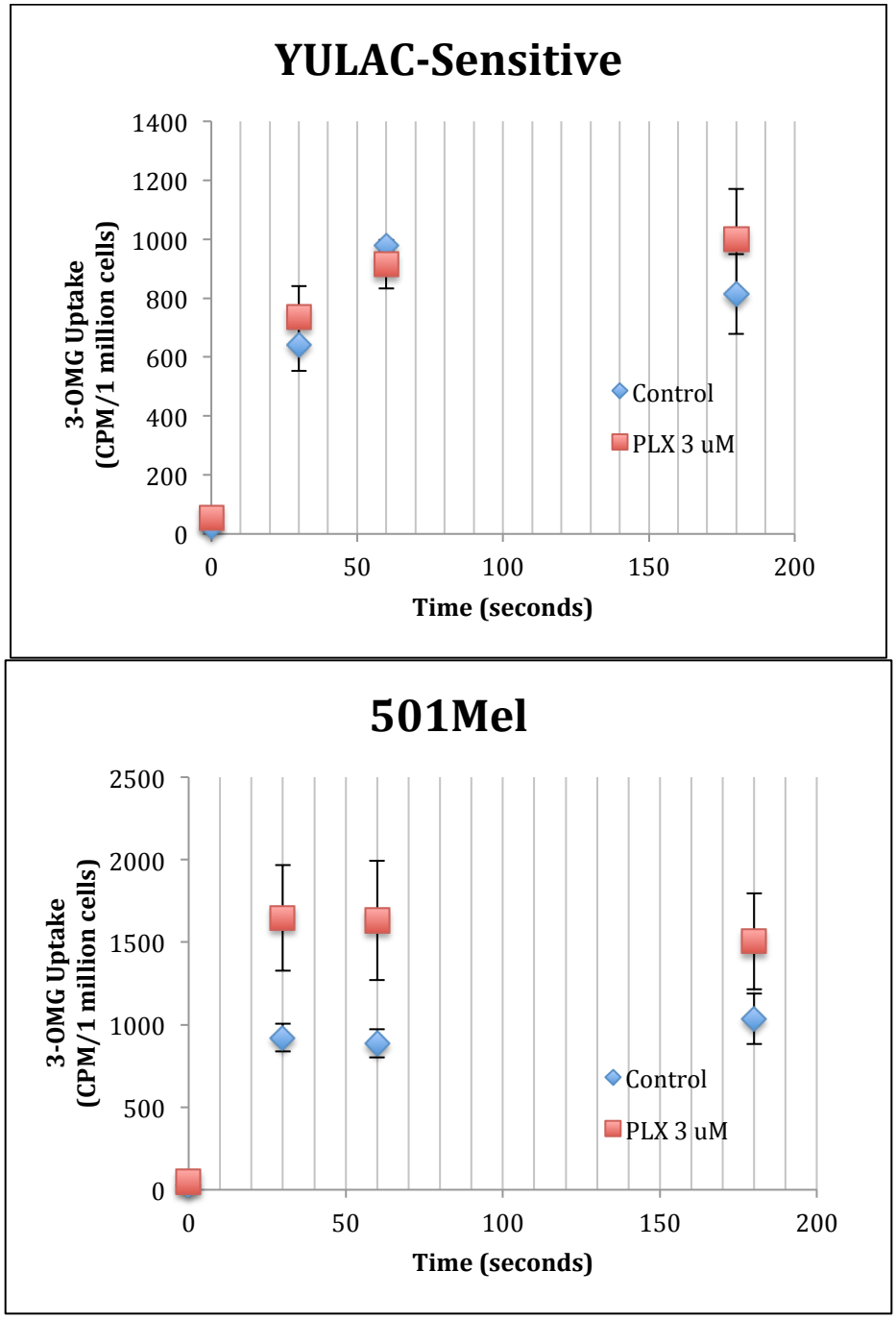

Figure 9. Time-course of tritiated 3-O-methylglucose uptake in YULAC-sensitive and 501Mel (resistant) human melanoma cell lines treated with vemurafenib for 72 hours. The YULAC-sensitive line showed no change in the level of surface transporters, as evidenced by the equal kinetics of 3-O-MG uptake between treated and control. 501Mel showed an increase in the level of glucose transporters, as evidenced by the increase in 3-O-MG uptake at 30 and 60 seconds (p-value<0.5).

Cell labeling

Labeling cells with ^{13}C-glucose followed by quantification of proportion of labeled metabolites, allows for the creation of a metabolic profile and for evaluation of flux. The YULAC-sensitive line showed decreased flux of ^{13}C through glycolysis to lactate and alanine with treatment consisting of 3 µM PLX4032. This decrease in flux was much less marked in the YULAC-resistant line. The production of lactate and phosphoglyceraldehyde were slightly increased in the 501Mel cell lines. There were no significant changes in the level of metabolites in the tricarboxylic acid cycle. Evaluation of glutamine levels is out of the scope of this thesis.

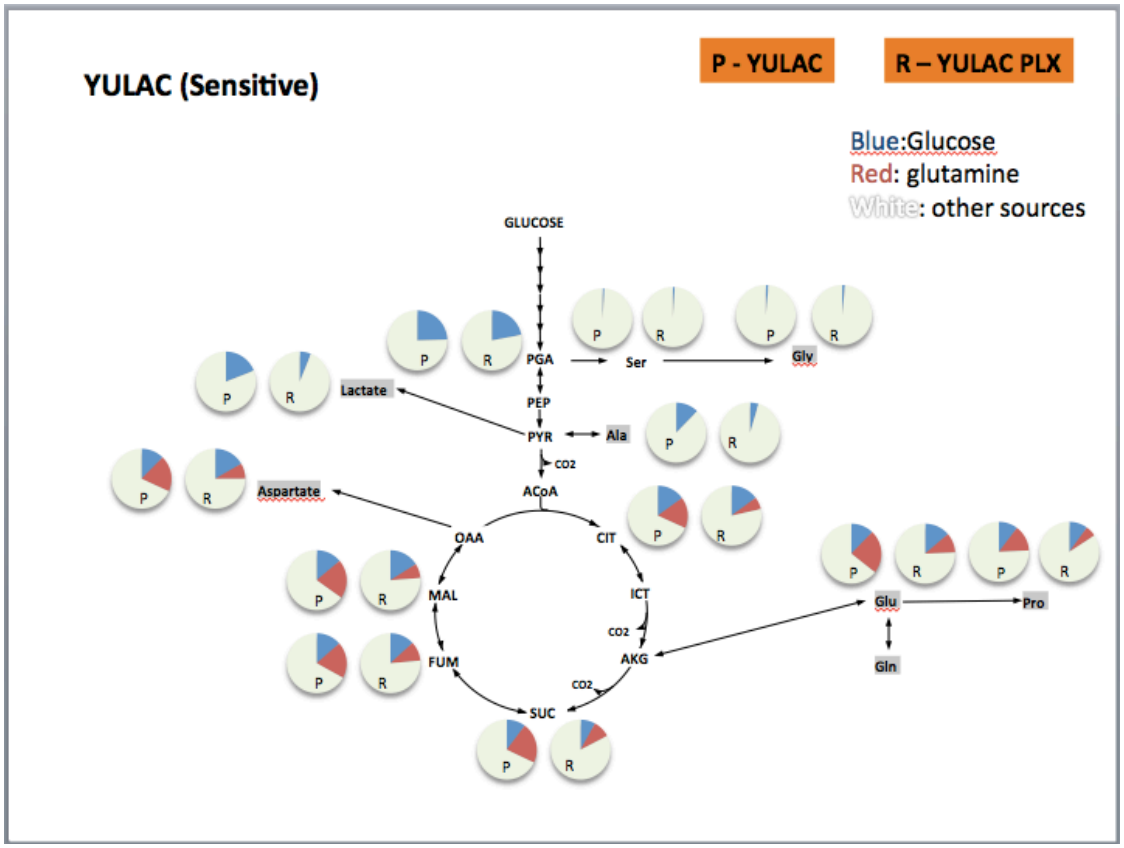

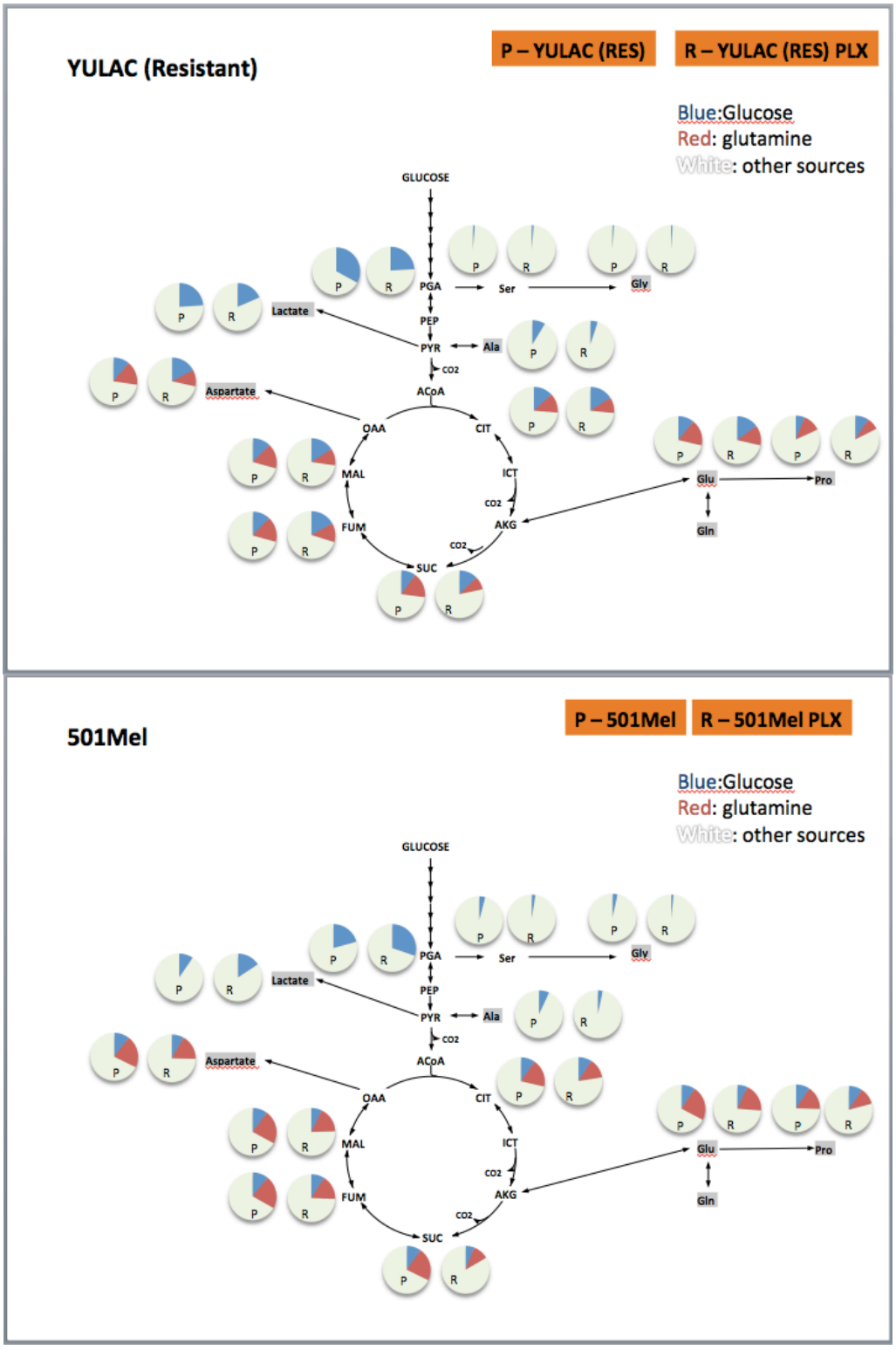

Figure 10. Metabolic profile of YULAC-sensitive, -resistant, and 501Mel before and after treatment with vemurafenib. The YULAC-sensitive line shows a decrease in the level of lactate with treatment, indicating decreased flux through glycolysis and possibly increased flux through the TCA cycle for oxidative phosphorylation. A concomitant increase in TCA cycle metabolites, however, was not observed. Lactate levels decreased slightly in YULAC-resistant and increased in 501Mel.

DISCUSSION

The effect of kinase inhibitors on cell metabolism has previously been studied. In particular, imatinib has been shown to decrease glucose uptake in BCR-ABL-positive cells and inhibit glycolysis[47]. Gefitinib, an EGFR receptor inhibitor, has been shown to inhibit glucose uptake in non-small cell lung cancer cell lines[44]. This study now shows that vemurafenib, a serine threonine kinase inhibitor, decreases glucose uptake by what appears to be a hexokinase-dependent mechanism and that this decrease in uptake may be important for the mechanism of action of the drug. The first set of data shows that treatment of sensitive cell lines (YULAC-sensitive, YUCOT, YURIF, YUKOLI) results in decreased glucose uptake whereas treatment of acquired or intrinsically resistant cell lines (501Mel, YULAC-resistant, YUKSI) does not. As confirmed by automatic trypan blue assay (Cell Countess), the decrease in uptake is not accompanied by a significant decrease in cell death (data not shown), indicating the result is not due to increased cell death in the treated samples. Interestingly, the inhibitory effect of vemurafenib on glucose uptake in the YULAC cell line is lost in the resistant counterpart, suggesting that glucose uptake may play an important role in the mechanism of resistance to vemurafenib. The decrease in uptake occurs between 7 and 9 hours in the YULAC sensitive cell line. The time course of uptake decrease points toward particular mechanisms. An immediate decrease in uptake would indicate a fast mechanism, such as phosphorylation of the transporters with subsequent blockage of the transport pore, is taking place. A delayed decrease, as was observed in this case, points toward a slow mechanism, such as downregulation of DNA transcription or alteration of translational efficiency.

The Braf/Pten mouse model was used to investigate glucose uptake in vivo. The melanoma tumor that forms in this model harbors a $Braf^{V600E}$ mutation and a PTEN deletion. PTEN is an inhibitor of phosphoinositide-3-kinase, a key regulator of the PI3K-mTOR pathway of cell metabolism. The absence of decreased glucose uptake in the tumor after 7, 14, 21, and 28 days of treatment might indicate the genetic makeup of the tumor renders the model resistant to decreases in glucose uptake. The absence of PTEN, theoretically, leaves the PI3K-mTOR pathway without its main negative regulator, possibly allowing glucose uptake to continue despite BRAF inhibition. Interestingly, treatment with PLX4720 reduces tumor growth in these mice. This might indicate a decoupling of growth arrest, through inhibition of cell proliferation via BRAF blockage, and glucose uptake, through lack of negative feedback via PTEN in the PI3K-mTOR pathway.

A decrease in glucose uptake can occur by either an effect on facilitative glucose transporters on the surface of the cell or by an effect on the intracellular hexokinase enzymes. The transporters allow passage of glucose into the cell. Hexokinase phosphorylates glucose to form glucose-6-phosphate and traps the compound inside the cell. The effect may be at the transcriptional (mRNA), translational (protein), or post-transcriptional level (protein modifications). More than one mechanism may be taking place. For example, non-small cell lung cancer cell lines show decreased FDG uptake by translocation of GLUT3 transporters from the plasma membrane to the cytosol and a modest decrease in hexokinase activity[44]. GLUT3, also known as the neuronal-type glucose transporter because of its preponderance in cells of the nervous system, has a higher affinity for glucose than GLUT1,-2, or -4 and has at least a fivefold greater

transport capacity than GLUT1 and -4[48]. These properties and the neural origin of melanocytes, namely neural crest cells, make GLUT3 a good candidate for the increased glucose uptake observed in melanoma cell lines. So far, however, the results do not confirm this hypothesis. In the case of chronic myelogenous leukemia, the decrease in glucose uptake observed with imatinib treatment is caused by intracellular translocation of GLUT1 transporters from the plasma membrane. Quantitative PCR showed changes in mRNA levels of GLUT1, GLUT3, HK1, HK2, and HK3 but these were within the margin of error. This indicates that although the time course is consistent with a transcriptional event, other mechanisms are taking place.

A hexokinase activity assay revealed that treatment with vemuferanib results in decreased hexokinase activity in the YULAC sensitive cell line but not in highly resistant 501Mel cell line, suggesting that vemurafenib decreases glucose uptake by a translational or post-translational mechanism at the level of hexokinase. For example, vemurafenib may inhibit translation of hexokinases. The three hexokinase isozymes differ in catalytic and regulatory properties as well as subcellular localization[49]. Hexokinase I appears to be constitutively expressed in a variety of cellular contexts. Hexokinases II is less abundant in normal tissues, but may be overexpressed in cancer. In terms of localization, HK1 and HK2 bind to the mitochondria and may be present in the cytoplasm whereas HK3 has a predominantly perinuclear localization in many cell types.

The glucose analog 3-O-methylglucose can enter the cell through glucose transporters but cannot be phosphorylated. As a result, a decrease in 3-O-MG in sensitive cell lines upon treatment with vemurafenib would indicate an effect at the level of the glucose transporters. No change was observed in 3-O-MG in YULAC-sensitive cell lines

suggesting glucose transporters do not translocate into cytoplasmic vesicles or become modified in a way that blocks their transport pores. The resistant cell line 501Mel, however, showed an increase in 3-OMG uptake indicating that vemurafenib might paradoxically enhance glucose uptake in this resistant line.

The metabolic profile of melanoma cell lines has previously been studied[46]. Specifically, all the melanoma cell lines in that study exhibited the Warburg phenomenon, which means they used more glucose and produced more lactate than melanocytes under aerobic conditions. Other changes observed in the study were increase in fermentation in both melanocytes and melanoma cells under hypoxic conditions, a phenomenon known as the Pasteur effect. In this thesis, the metabolic profile of melanoma cells was evaluated in the presence of vemurafenib. The global picture of glucose metabolism in sensitive and resistant lines that this experiment generated showed that vemurafenib decreases flux through glycolysis in the YULAC-sensitive but not in the YULAC-resistant line as evidenced by the drop in lactate levels. Interestingly, 501Mel shows a slight increase in lactate levels with vemurafenib treatment. This is consistent with the increase in 3-O-methylglucose inflow observed with treatment in the 501Mel line. Overall, these experiments support the hypothesis that vemurafenib induces a metabolic profile in melanoma cell lines that is limited in glycolysis, reversing the Warburg effect. The effect of vemurafenib on glutamine levels is out of the scope of this thesis.

Future directions for this study include the corroboration of glucose uptake time-course experiments with flow cytometry in vitro. While mRNA levels of the glucose transporter were unchanged, Westerns blots will be important to analyze variation in

protein levels. The localization of the glucose transporters might also be affected, despite the data that showed no change in 3-O-MG uptake in the YULAC-sensitive line, and will be studied with confocal microscopy. Given the variety of glucose transporters and hexokinases, siRNA or shRNA experiments would be useful in evaluating the contribution of each protein to glucose uptake.

REFERENCES

1. Miller AJ, Mihm MC. Mechanisms of disease - Melanoma. New England Journal of Medicine 2006;355:51-65.
2. Gill M, Celebi JT. B-RAF and melanocytic neoplasia. J Am Acad Dermatol 2005;53:108-14.
3. Davies H, Bignell GR, Cox C, et al. Mutations of the BRAF gene in human cancer. Nature 2002;417:949-54.
4. Hocker T, Tsao H. Ultraviolet radiation and melanoma: a systematic review and analysis of reported sequence variants. Hum Mutat 2007;28:578-88.
5. Carr J, Mackie RM. Point mutations in the NRAS oncogene in malignant melanoma and congenital naevi. Br J Dermatol 1994;131:72-7.
6. Herlyn M, Satyamoorthy K. Activated ras. Yet another player in melanoma? Am J Pathol 1996;149:739-44.
7. Reifenberger J, Knobbe CB, Sterzinger AA, et al. Frequent alterations of Ras signaling pathway genes in sporadic malignant melanomas. Int J Cancer 2004;109:377-84.
8. Poynter JN, Elder JT, Fullen DR, et al. BRAF and NRAS mutations in melanoma and melanocytic nevi. Melanoma Res 2006;16:267-73.
9. Demunter A, Stas M, Degreef H, De Wolf-Peeters C, van den Oord JJ. Analysis of N- and K-ras mutations in the distinctive tumor progression phases of melanoma. J Invest Dermatol 2001;117:1483-9.
10. Jiveskog S, Ragnarsson-Olding B, Platz A, Ringborg U. NRAS mutations are common in melanomas from sun-exposed skin of humans but rare in mucosal membranes or unexposed skin. J Invest Dermatol 1998;111:757-61.
11. van Elsas A, Zerp SF, van der Flier S, et al. Relevance of ultraviolet-induced NRAS oncogene point mutations in development of primary human cutaneous melanoma. Am J Pathol 1996;149:883-93.
12. Serrano M, Blasco MA. Putting the stress on senescence. Curr Opin Cell Biol 2001;13:748-53.
13. Collado M, Serrano M. The power and the promise of oncogene-induced senescence markers. Nat Rev Cancer 2006;6:472-6.
14. Campisi J. Senescent cells, tumor suppression, and organismal aging: good citizens, bad neighbors. Cell 2005;120:513-22.
15. Hollstein M, Sidransky D, Vogelstein B, Harris CC. p53 mutations in human cancers. Science 1991;253:49-53.
16. Ruas M, Peters G. The p16INK4a/CDKN2A tumor suppressor and its relatives. Biochim Biophys Acta 1998;1378:F115-77.
17. Sharpless NE, DePinho RA. The INK4A/ARF locus and its two gene products. Curr Opin Genet Dev 1999;9:22-30.
18. Michaloglou C, Vredeveld LC, Soengas MS, et al. BRAFE600-associated senescence-like cell cycle arrest of human naevi. Nature 2005;436:720-4.
19. Gray-Schopfer VC, Cheong SC, Chong H, et al. Cellular senescence in naevi and immortalisation in melanoma: a role for p16? Br J Cancer 2006;95:496-505.

20. Huot TJ, Rowe J, Harland M, et al. Biallelic mutations in p16(INK4a) confer resistance to Ras- and Ets-induced senescence in human diploid fibroblasts. Mol Cell Biol 2002;22:8135-43.
21. Dhomen N, Reis-Filho JS, da Rocha Dias S, et al. Oncogenic Braf induces melanocyte senescence and melanoma in mice. Cancer Cell 2009;15:294-303.
22. Hazen BP, Bhatia AC, Zaim T, Brodell RT. The clinical diagnosis of early malignant melanoma: expansion of the ABCD criteria to improve diagnostic sensitivity. Dermatol Online J 1999;5:3.
23. Balch CM, Gershenwald JE, Soong SJ, et al. Final version of 2009 AJCC melanoma staging and classification. J Clin Oncol 2009;27:6199-206.
24. Pollack LA, Li J, Berkowitz Z, et al. Melanoma survival in the United States, 1992 to 2005. J Am Acad Dermatol 2011;65:S78-86.
25. Atkins MB, Kunkel L, Sznol M, Rosenberg SA. High-dose recombinant interleukin-2 therapy in patients with metastatic melanoma: long-term survival update. Cancer J Sci Am 2000;6 Suppl 1:S11-4.
26. Hodi FS, O'Day SJ, McDermott DF, et al. Improved survival with ipilimumab in patients with metastatic melanoma. N Engl J Med 2010;363:711-23.
27. Robert C, Thomas L, Bondarenko I, et al. Ipilimumab plus dacarbazine for previously untreated metastatic melanoma. N Engl J Med 2011;364:2517-26.
28. Flaherty KT, Puzanov I, Kim KB, et al. Inhibition of mutated, activated BRAF in metastatic melanoma. N Engl J Med 2010;363:809-19.
29. Paraiso KH, Fedorenko IV, Cantini LP, et al. Recovery of phospho-ERK activity allows melanoma cells to escape from BRAF inhibitor therapy. Br J Cancer 2010;102:1724-30.
30. Nazarian R, Shi H, Wang Q, et al. Melanomas acquire resistance to B-RAF(V600E) inhibition by RTK or NRAS upregulation. Nature 2010;468:973-7.
31. Tsao H, Atkins MB, Sober AJ. Management of cutaneous melanoma. N Engl J Med 2004;351:998-1012.
32. Young K, Minchom A, Larkin J. BRIM-1, -2 and -3 trials: improved survival with vemurafenib in metastatic melanoma patients with a BRAF(V600E) mutation. Future Oncol 2012;8:499-507.
33. Chapman PB, Hauschild A, Robert C, et al. Improved survival with vemurafenib in melanoma with BRAF V600E mutation. N Engl J Med 2011;364:2507-16.
34. Hanahan D, Weinberg RA. Hallmarks of cancer: the next generation. Cell 2011;144:646-74.
35. DeBerardinis RJ, Lum JJ, Hatzivassiliou G, Thompson CB. The biology of cancer: metabolic reprogramming fuels cell growth and proliferation. Cell Metab 2008;7:11-20.
36. Hsu PP, Sabatini DM. Cancer cell metabolism: Warburg and beyond. Cell 2008;134:703-7.
37. Jones RG, Thompson CB. Tumor suppressors and cell metabolism: a recipe for cancer growth. Genes Dev 2009;23:537-48.
38. Hassanein M, Weidow B, Koehler E, et al. Development of high-throughput quantitative assays for glucose uptake in cancer cell lines. Mol Imaging Biol 2011;13:840-52.

39. Vander Heiden MG. Targeting cancer metabolism: a therapeutic window opens. Nat Rev Drug Discov 2011;10:671-84.
40. Inoki K, Corradetti MN, Guan KL. Dysregulation of the TSC-mTOR pathway in human disease. Nat Genet 2005;37:19-24.
41. McArthur GA, Puzanov I, Amaravadi R, et al. Marked, homogeneous, and early [18F]fluorodeoxyglucose-positron emission tomography responses to vemurafenib in BRAF-mutant advanced melanoma. J Clin Oncol 2012;30:1628-34.
42. Dankort D, Curley DP, Cartlidge RA, et al. Braf(V600E) cooperates with Pten loss to induce metastatic melanoma. Nat Genet 2009;41:544-52.
43. Yamamoto N, Ueda M, Sato T, et al. Measurement of glucose uptake in cultured cells. Curr Protoc Pharmacol 2011;Chapter 12:Unit 12 4 1-22.
44. Su H, Bodenstein C, Dumont RA, et al. Monitoring tumor glucose utilization by positron emission tomography for the prediction of treatment response to epidermal growth factor receptor kinase inhibitors. Clin Cancer Res 2006;12:5659-67.
45. Wei LH, Su H, Hildebrandt IJ, Phelps ME, Czernin J, Weber WA. Changes in tumor metabolism as readout for Mammalian target of rapamycin kinase inhibition by rapamycin in glioblastoma. Clin Cancer Res 2008;14:3416-26.
46. Scott DA, Richardson AD, Filipp FV, et al. Comparative metabolic flux profiling of melanoma cell lines: beyond the Warburg effect. J Biol Chem 2011;286:42626-34.
47. Kominsky DJ, Klawitter J, Brown JL, et al. Abnormalities in glucose uptake and metabolism in imatinib-resistant human BCR-ABL-positive cells. Clin Cancer Res 2009;15:3442-50.
48. Simpson IA, Dwyer D, Malide D, Moley KH, Travis A, Vannucci SJ. The facilitative glucose transporter GLUT3: 20 years of distinction. Am J Physiol Endocrinol Metab 2008;295:E242-53.
49. Wilson JE. Isozymes of mammalian hexokinase: structure, subcellular localization and metabolic function. J Exp Biol 2003;206:2049-57.